Nematic liquid-crystal alignment on stripe-patterned substrates

C. Anquetil-Deck
Laboratoire Chimie Provence, UMR 6264, University of Aix-Marseille I, Avenue Escadrille Normandie-Niemen, 13397 Marseille Cedex 20, France

D. J. Cleaver*
Materials and Engineering Research Institute, Sheffield Hallam University, City Campus, Howard Street, Sheffield S1 1WB, United Kingdom

(Received 10 May 2010; revised manuscript received 19 August 2010; published 27 September 2010)

Here, we use molecular simulation to consider the behavior of a thin nematic film confined between two identical nanopatterned substrates. Using patterns involving alternating stripes of homeotropic-favoring and homogeneous-favoring substrates, we investigate the influence of the relative stripe width and the film thickness. From this, we show that the polar anchoring angle can be varied continuously from planar to homeotropic by appropriate tuning of these parameters. For very thin films with equal stripe widths, we observe orientational bridging, the surface patterning being written in domains which traverse the nematic film. This dual-bridging-domain arrangement breaks down with increase in film thickness, however, being replaced by a single tilted monodomain. Strong azimuthal anchoring in the plane of the stripe boundaries is observed for all systems.

DOI: 10.1103/PhysRevE.82.031709 PACS number(s): 61.30.Hn, 07.05.Tp

I. INTRODUCTION

The means by which the director orientation of a bulk liquid crystal (LC) is imposed by its confining substrates is called anchoring [1]. The vast majority of LC switching devices rely in some way on anchoring to set their dynamic and equilibrium properties. Substrate-controlled director alignment is a device-scale effect which results from the interplay of the microscopic orientational and positional degrees of freedom of the LC molecules located in the proximity of their confining surfaces. Traditional routes to establishing desired anchoring behaviors include substrate rubbing and various photoalignment approaches such as light-induced *cis-trans* isomerization and photodegradation. The molecular mechanisms by which these operate are, though, poorly understood.

More recently, developments have been made in utilizing spatially inhomogeneous substrates to control LC anchoring properties. The most obvious systems that fall into this category are the structurally inhomogeneous substrates employed in the zenithally bistable nematic [2] and postaligned bistable nematic [3] device geometries. In these, long-lived bistability is achieved due to the ability of the structured substrates to stabilize optically distinct continuous and defect states. An alternative, but monostable, alignment approach based on steric patterning utilizes regular scratch arrays, etched using atomic force microscope tips [4].

Chemical patterning offers an alternative approach by which to impose substrate inhomogeneity in LC systems. The concept of simultaneous alignment of azimuthal and polar orientation of LCs by chemical nanopatterns was the subject of early experimental work [5–7]. Subsequently, Lee and Clark studied the alignment properties of nematic LCs on surfaces containing homeotropic and planar alignment areas on the same substrate. They showed that the polar orientation depends on the ratio of the homeotropic and planar surface-potential areas, while the LC azimuthally orients along the direction of the stripes [10]. In 2005, Park and co-workers [8,9] also investigated systems with competing alignment regions. Alternative systems utilizing alkanethiol self-assembled monolayers (SAMs) on gold were developed by the groups of Abbott [11] and Evans [12]. Using microcontact printing, these systems are able to achieve highly reproducible surface features with periodicities of tens of microns. Square, circular, and stripe patterns written on these length scales have, thus, been observed using optical microscopy in crossed polarizer setups. An alternative approach, employing selective ultraviolet irradiation of SAMs, has achieved LC-aligning stripe patterns on the submicron scale [13].

In Ref. [14], we contributed the simulation aspects of a joint experimental and simulation study of LC alignment at a single-patterned substrate. In this, it was shown that a range of patterned SAMs can be used to control LC alignment states and domains. For stripe patterns, the LC was found to align parallel to the stripe boundaries for both nanoscale simulation features and micron-scale experimental systems. Indeed, despite the significantly different length scales involved, the qualitative behavior seen in simulations of generic molecular models confined using a striped interface proved entirely consistent with the experimental observations. Specifically, on undergoing isotropic to nematic ordering, all systems proved to be dominated by the homeotropic-aligning substrate regions *at* the ordering transition, the influence of the planar-aligning regions only becoming apparent well into the nematic.

In this paper, we follow up on our previous single-patterned substrate results by concentrating on the behavior of confined LC film systems with stripe patterns on both of their substrates and study the influence of the film thickness and the relative proportions of homeotropic and planar align-

*d.j.cleaver@shu.ac.uk

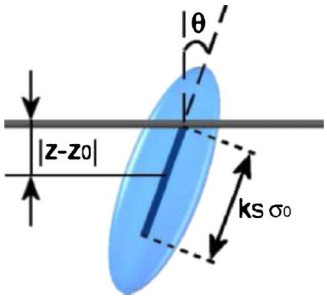

FIG. 1. (Color online) Schematic representation of the geometry used for the HNW particle-substrate interaction [16].

ment areas on the substrates. In Sec. II we present our model system and describe the simulation methodology employed. Section III contains results obtained from an initial thin-film system with equal stripe widths. In Secs. IV and V, we examine the influence of relative stripe width and of film thickness, respectively. Finally, in Sec. VI, we draw some conclusions.

II. MODEL AND SIMULATION DETAILS

We have performed a series of Monte Carlo (MC) simulations of rod-shaped particles confined in slab geometry between two planar walls. Interparticle interactions have been modeled through the hard Gaussian overlap (HGO) potential [15]. Here, the dependence of the interaction potential ν^{HGO} on $\hat{\mathbf{u}}_i$ and $\hat{\mathbf{u}}_j$, the orientations of particles i and j, and $\hat{\mathbf{r}}_{ij}$, the interparticle unit vector, is

$$\nu^{\mathrm{HGO}} = \begin{cases} 0 & \text{if } r_{ij} \geq \sigma(\hat{\mathbf{r}}_{ij}, \hat{\mathbf{u}}_i, \hat{\mathbf{u}}_j) \\ \infty & \text{if } r_{ij} < \sigma(\hat{\mathbf{r}}_{ij}, \hat{\mathbf{u}}_i, \hat{\mathbf{u}}_j), \end{cases}$$

where $\sigma(\hat{\mathbf{r}}_{ij}, \hat{\mathbf{u}}_i, \hat{\mathbf{u}}_j)$, the contact distance, is given by

$$\sigma(\hat{\mathbf{r}}_{ij}, \hat{\mathbf{u}}_i, \hat{\mathbf{u}}_j) = \sigma_0 \left\{ 1 - \frac{\chi}{2} \left[\frac{(\hat{\mathbf{r}}_{ij} \cdot \hat{\mathbf{u}}_i + \hat{\mathbf{r}}_{ij} \cdot \hat{\mathbf{u}}_j)^2}{1 + \chi(\hat{\mathbf{u}}_i \cdot \hat{\mathbf{u}}_j)} + \frac{(\hat{\mathbf{r}}_{ij} \cdot \hat{\mathbf{u}}_i - \hat{\mathbf{r}}_{ij} \cdot \hat{\mathbf{u}}_j)^2}{1 - \chi(\hat{\mathbf{u}}_i \cdot \hat{\mathbf{u}}_j)} \right] \right\}^{-1/2}. \quad (1)$$

The parameter χ is set by the particle length to breadth ratio $\kappa = \sigma_{end}/\sigma_{side}$ via

$$\chi = \frac{\kappa^2 - 1}{\kappa^2 + 1}. \quad (2)$$

Particle-substrate interactions have been modeled using the hard needle-wall (HNW) potential [16]. In this, the particles do not interact directly with the surfaces. Rather the surface interaction is achieved by considering a hard axial needle of length $\sigma_0 k_s$ placed at the center of each particle (see Fig. 1). This gives an interaction

$$\nu^{\mathrm{HNW}} = \begin{cases} 0 & \text{if } |z_i - z_0| \geq \sigma_w(\hat{\mathbf{u}}_i) \\ \infty & \text{if } |z_i - z_0| < \sigma_w(\hat{\mathbf{u}}_i), \end{cases}$$

where z_0 represents the location of a substrate and

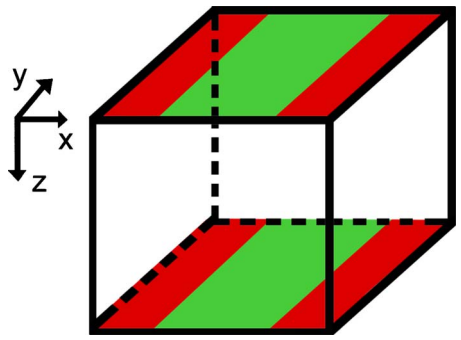

FIG. 2. (Color online) Schematic representation of stripe-patterned systems with alternating homeotropic-inducing (red or dark) and planar-inducing (green or light) substrate regions.

$$\sigma_w(\hat{\mathbf{u}}_i) = \tfrac{1}{2}\sigma_0 k_s \cos(\theta_i). \quad (3)$$

Here, k_s is the dimensionless needle length and $\theta_i = \arccos(u_{i,z})$ is the angle between the substrate normal and the particle's orientation vector. For small k_s, the homeotropic arrangement has been shown to be stable, whereas planar anchoring is favored for long k_s [16]. Furthermore, despite its simplicity, the HNW potential has been found to exhibit qualitatively identical behavior to that obtained using more complex particle-substrate potentials [17]. Here, by imposing variation in k_s across the two boundary walls, we investigate the effects of molecular-scale substrate patterning on LC anchoring. The results presented in Secs. III and IV have been obtained for systems of 864, $\kappa=3$ HGO particles confined between two stripe-patterned substrates. In these systems, the substrates were separated by a distance $L_z = 4\kappa\sigma_0$, periodic boundary conditions being imposed in the x and y directions.

On each substrate, k_s was set to a homeotropic-aligning value ($k_s=0$) for a stripe portion of its area and a planar value ($k_s=3$) for the remainder. Here, sharp boundaries have been imposed between the different alignment regions, the stripe boundaries running parallel to the y axis of the simulation box. The patterns on the top and bottom surfaces have been kept in perfect registry with one another, as shown in the schematic diagram (Fig. 2). Each system has been initialized at low density and gently compressed by decreasing the box dimensions L_x and L_y. At each density, run lengths of 1×10^6 MC sweeps (where one sweep represents one attempted move per particle) were performed, averages and profiles being accumulated for the final 500 000 sweeps.

Detailed analysis was performed by dividing stored system configurations into 100 equidistant constant-z slices and calculating averages of relevant observables in each slice. This yielded profiles of quantities, such as number density, $\rho^*(z)$, from which structural changes could be assessed. Orientational order profiles were also measured, particularly

$$Q_{zz}(z) = \frac{1}{N(z)} \sum_{i=1}^{N(z)} \left(\frac{3}{2} u_{i,z}^2 - \frac{1}{2} \right), \quad (4)$$

which measures variation across the confined films of orientational order measured with respect to the substrate normal. Here, $N(z)$ is the instantaneous occupancy of the relevant

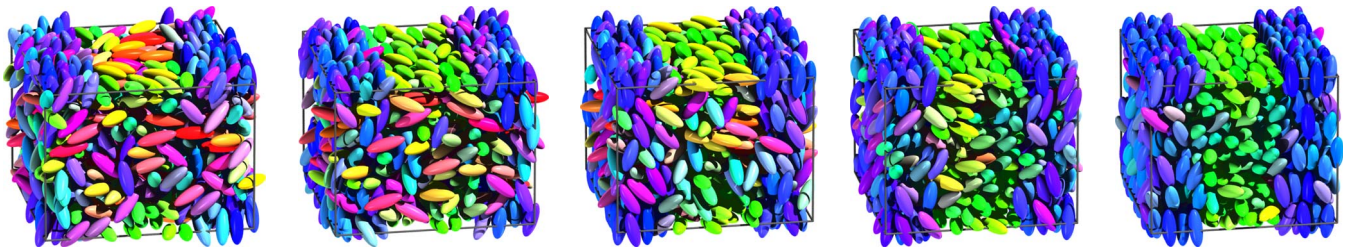

FIG. 3. (Color online) Snapshots of the 50:50 stripe-patterned system at a series of reduced densities. Color coding is used to indicate particle orientation.

slice. We have also further subdivided the system to assess lateral inhomogeneities induced by the patterning.

III. INITIAL STRIPE-PATTERNED SYSTEM

In the first system considered here, the proportions of the homeotropic and planar alignment regions were both set to 50%. The outcomes of these first striped system simulations are summarized by the snapshots shown in Fig. 3. Several remarks emerge from these. At low density ($\rho^*=0.3$), the central region of the film remains relatively disordered, but the near-surface regions adopt orientations consistent with their imposed k_s values [Fig. 3(a)]. Even at the relatively low density of $\rho^*=0.32$, the particles adjacent to the $k_s=3$ stripes show a marked preference to lie parallel to the stripe boundaries [Fig. 3(b)]. With increase in density, orientational order appears to develop between the $k_s=0$ surface regions [Fig. 3(c)], while the other central region of the film (confined between $k_s=3$ substrate regions) remains relatively disordered. At the reduced density $\rho^*=0.39$ [Fig. 3(e)], both midfilm regions appear orientationally ordered. However, rather than forming a monodomain, the orientations adopted in the two central regions are apparently the same as those of the particles aligned at the corresponding substrate regions: the stripe pattern is, thus, written across the film in domains in an interesting manifestation of bridging [18,19].

In the light of these observations, we have analyzed the behavior of this system by calculating two sets of profiles of key observables for each system; for analysis purposes, each simulated system is split into two according to the imposed substrate pattern. In this, individual particles have been allocated to homeotropic-confined or homogeneous-confined regions according to their x coordinates. While there is further x dependence within these two regions, we have found that the dominant inhomogeneity is the orientational discontinuity apparent between the domains observed in Fig. 3.

The density profiles depicted in Fig. 4(a) show adsorption characteristics for the portion of the film confined between the homeotropic substrate regions. These indicate that increasing the density leads to formation of surface layers with a periodicity of $\simeq 2.5\sigma_0$. This distance corresponds approximately to the particle length. Figure 4(b) shows that, in the planar-confined part of the film, conversely, the layers formed have a periodicity of about σ_0. In this region, then, it appears that the molecules are arranged side to side close to the substrates but that the positional structure is smeared out in the central region.

To characterize this behavior further, we have calculated the average director for particles in the central 50% of each half of our system. We denote the director components along the simulation box axes as n_x, n_y, and n_z. The angles θ_x, θ_y, and θ_z formed between the box axes and the director can then be readily determined by inversion of these direction cosines. Characteristic behavior of the two sets of n_x, n_y, and n_z is shown in Fig. 5 as simulation "time" series calculated for 500 configurations in the production sequence of the $\rho^*=0.4$ run.

Figure 5(a) shows that the portion of the film subjected to homeotropic alignment has its largest director component aligned along the z axis, apparently, corresponding to homeotropic anchoring. In the other portion of the film, conversely, the largest component is aligned along the y direction [Fig. 5(b)]. To determine the tilt angles in the two

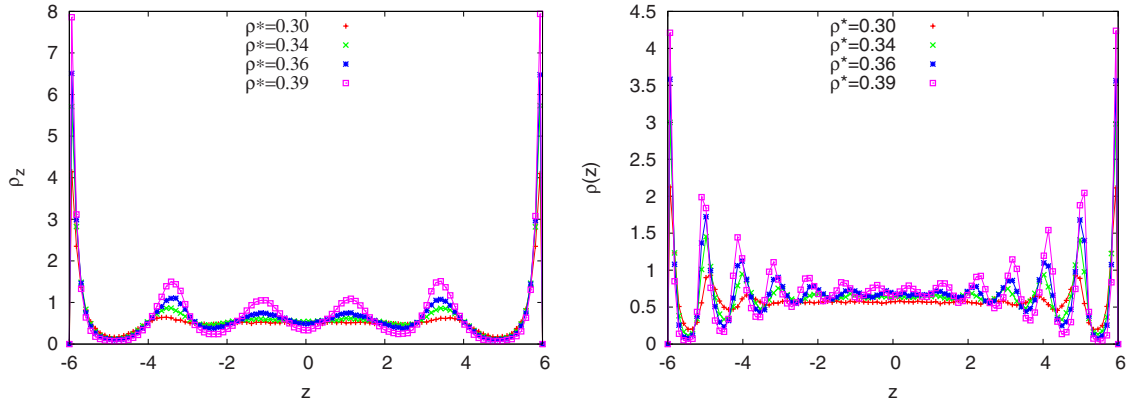

FIG. 4. (Color online) Density profiles for the 50:50 stripe-patterned system at different average densities ρ^*.

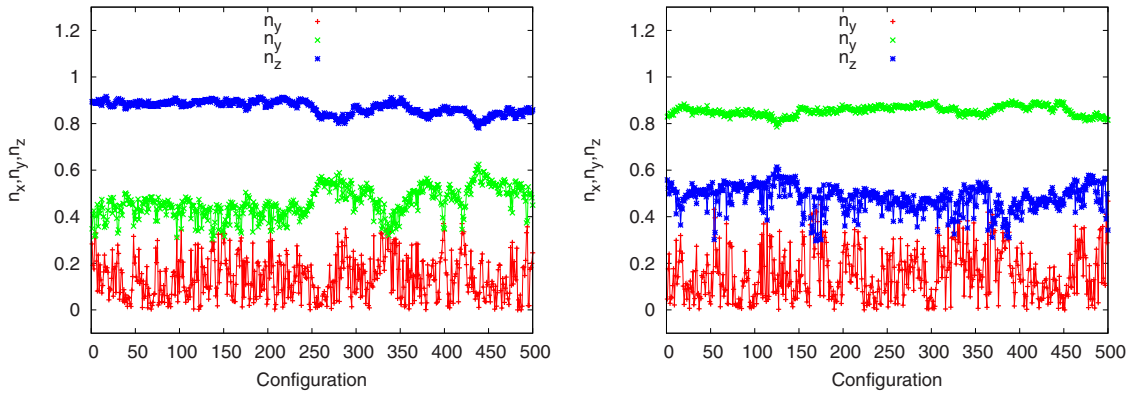

FIG. 5. (Color online) Time series showing the director components for 500 configurations in the $\rho^*=0.4$ production run.

regions, we use the angle measured with respect to the largest component in each region since this suffers least from noise. From this, we obtain angles of $\theta_z=29°$ in the homeotropic-confined region and $\theta_y=28°$ in the planar-confined region. These director tilt angles are significantly different from one another but are also very different from the zero values expected for classic homeotropic and planar anchorings. Thus, they indicate that the initial inference drawn from the snapshots (Fig. 3), that the confined film is split into homeotropic and planar portions, may not be fully correct.

A more complete understanding of the orientational aspects of the surface induced ordering in this system can be obtained from profiles of the three diagonal order tensor components Q_{ii}. For perfect homeotropic anchoring, Q_{zz} should tend to 1, with Q_{xx} and Q_{yy} going to −0.5. At low density, Fig. 6 shows that both Q_{xx} and Q_{yy} are negative close to the homeotropic wall regions. On increasing the density, peaks appear in the bulk region and Q_{xx} drops to −0.4. However, the value of Q_{yy} stagnates at around −0.1. Figure 6(c) shows that, at low density, the corresponding Q_{zz} profile is zero in the midfilm region but positive close to the substrates, consistent with homeotropic order developing at the walls. On increasing the density, the midfilm Q_{zz} value increases, indicating onset of orientational order with significant alignment along the z axis. However, the average midfilm Q_{zz} value fails to exceed 0.5 at high densities. These profiles indicate, therefore, that the midfilm director has ho-

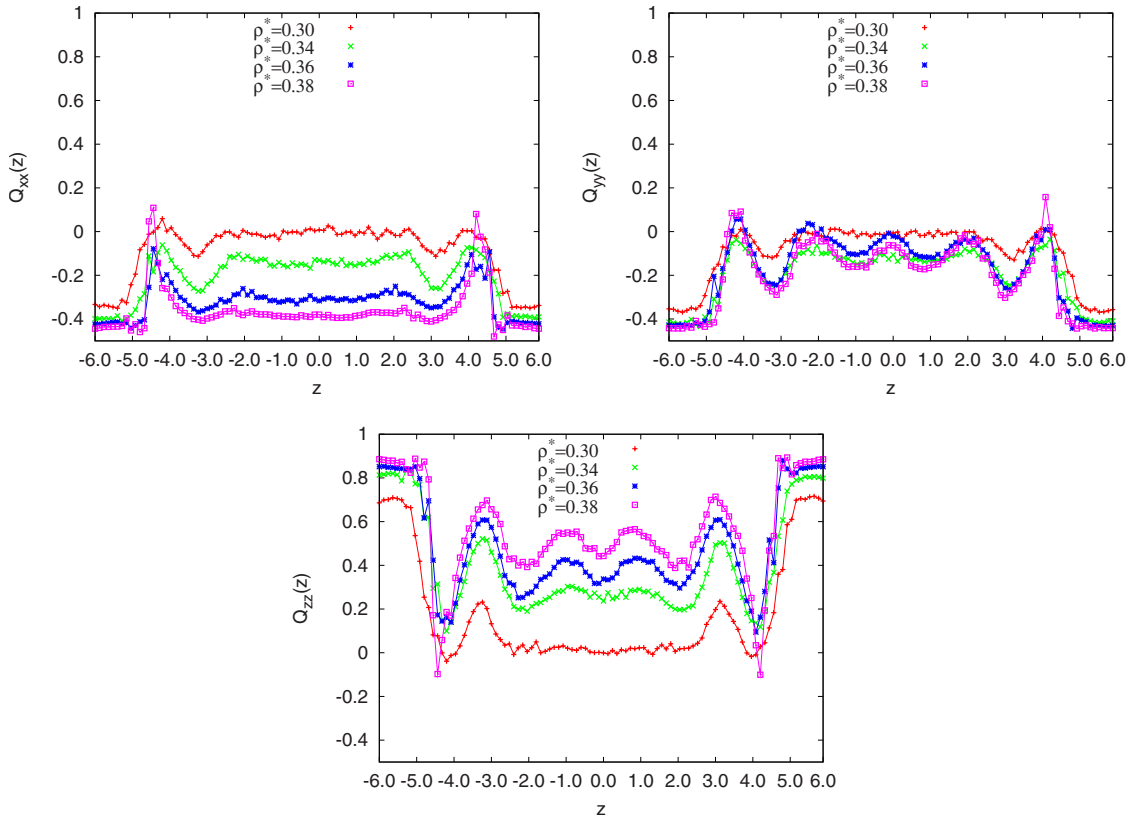

FIG. 6. (Color online) Density-dependent profiles of the diagonal components of the order tensor, homeotropic-confined region.

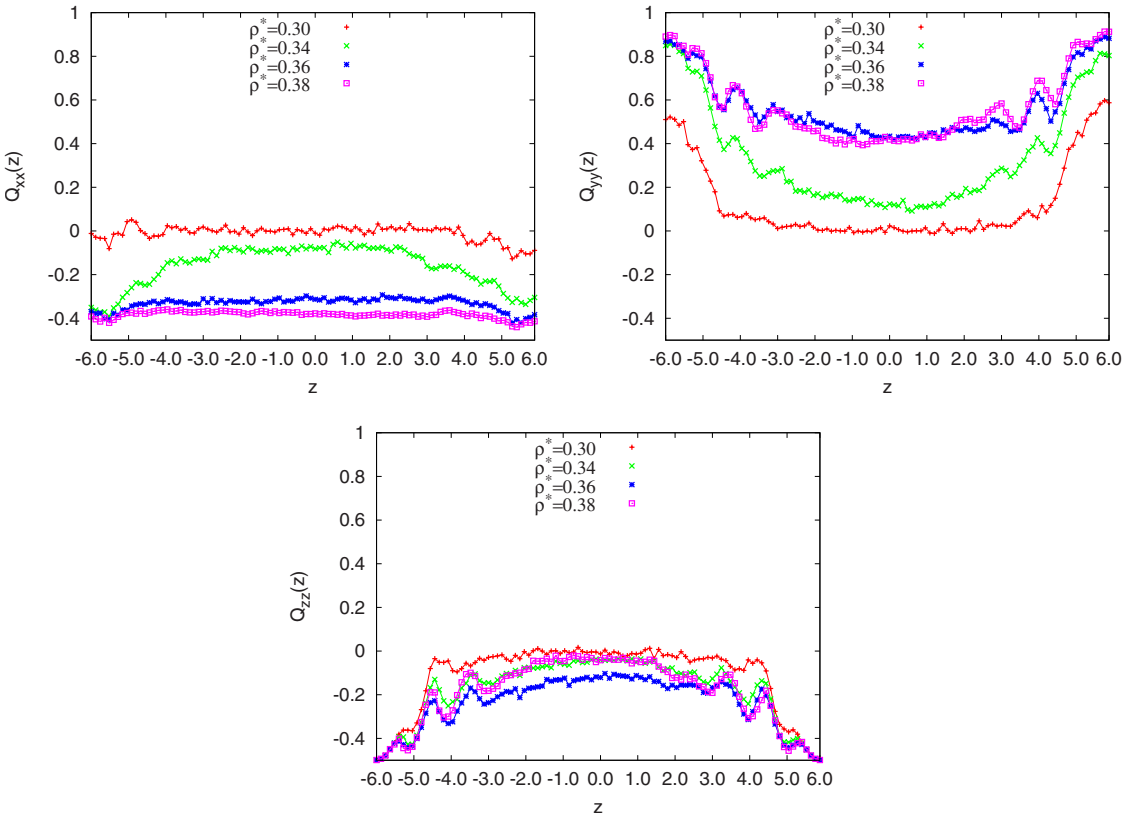

FIG. 7. (Color online) Density-dependent profiles of the diagonal components of the order tensor, planar-confined region.

meotropic character but, because the Q_{yy} value is well above −0.5, it is tilted in the yz plane.

In the planar-confined region, the behavior of these diagonal order tensor components shows some marked differences. At low density, Q_{xx} [Fig. 7(a)] is zero everywhere. As the density is increased, however, Q_{xx} rapidly becomes negative close to the walls and subsequently goes negative across the whole of the film. Thus, at high density ($\rho^*=0.38$), Q_{xx} is about −0.4 throughout. This indicates strong particle alignment perpendicular to the x axis, i.e., in the plane of the stripe boundaries. At low density, Q_{yy} [Fig. 7(b)] is positive close to the walls (∼0.5) and zero in the midfilm region. As the density is increased, Q_{yy} increases close to the wall (∼0.9) as well as in the bulk (∼0.5). This indicates that the average particle alignment has a significant component parallel to the y axis. Correspondingly, Q_{zz} [Fig. 7(c)] is negative close to the walls, indicating that the surface particles lie in the plane of the substrate. As the density is increased, negative Q_{zz} values are also seen midfilm but these only go down to −0.2. The implication of this combination of Q_{ii} behaviors is, again, that the average orientation in the midfilm is tilted.

We can confirm these tilts by considering the off-diagonal components $Q_{xy}(z)$ and $Q_{xz}(z)$. The latter (not shown) are found to be zero at all densities. In Fig. 8, we show that the off-diagonal component $Q_{yz}(z)$ is also zero throughout the

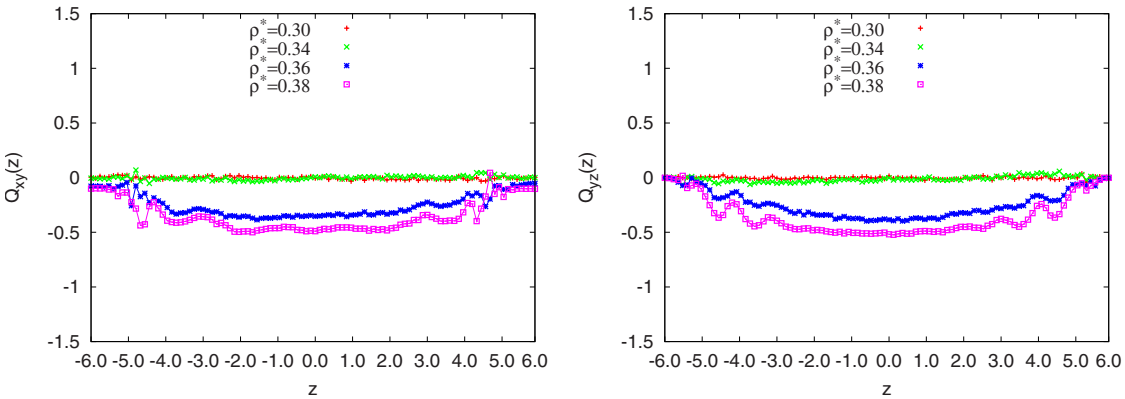

FIG. 8. (Color online) Density-dependent profiles of the off-diagonal component $Q_{yz}(z)$ of the order tensor for (a) homeotropic-confined region and (b) planar-confined region.

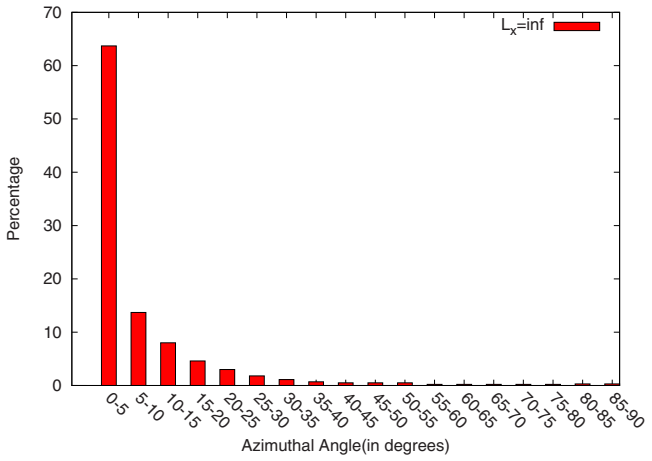

FIG. 9. (Color online) Histogram representing the particle azimuthal angle distribution in the planar surface region for the stripe-patterned system with 50% H and 50% P coverage on the surfaces, $\rho^*=0.39$.

film for $\rho^* \leq 0.36$. For ρ^* greater than 0.36, however $Q_{yz}(z)$ decreases and tends to −0.5 in both the planar-confined and the homeotropic-confined portions.

In the light of this fuller analysis, we can now draw some conclusions concerning this initial stripe-patterned substrates system. First, there is a strong tendency for the molecules to align in the plane of the stripe boundaries. Such behavior has been seen experimentally in systems of LCs adsorbed at stripe-patterned substrates (e.g., [14]). We quantify this effect in Fig. 9, which shows the particle azimuthal-angle distribution function obtained at a reduced density of 0.39. This is strongly peaked in the small azimuthal angle regime $0 \leq \phi \leq 5°$.

However, the issue of polar anchoring is slightly more complex. At first sight, Fig. 3 suggests that the surface patterns are written unmodified across the film. However, the more detailed analysis given above shows that, in fact, the midfilm regions are tilted, a different tilt being observed between each surface-coupling region. From this, it is apparent that the two domains identified from Fig. 3 have a negligible influence on one another. This leads to the midfilm director adopting a spatial variation in its y and z components, the x component remaining small throughout. One can, alternatively, envisage the possibility of a uniformly oriented bulk monodomain being a stable arrangement. Such behavior has been predicted previously at much larger length scales by Kondrat *et al.* [20]. They considered LCs adsorbed at striped substrates with finite-strength homeotropic and homogeneous anchoring regions. Where one set of stripes was much narrower than the other, the bulk nematic was found to adopt a spatially uniform configuration rather than a periodically distorted arrangement. In the following sections, we investigate the requirements for this alternative scenario by considering the sensitivity of these molecular systems to the relative surface coverage and the film thickness.

IV. INFLUENCE OF THE RELATIVE COVERAGE OF THE HOMEOTROPIC AND PLANAR SURFACE STRIPE REGIONS

In this section, we assess the influence of the relative sizes of the homeotropic (H) and planar (P) striped alignment regions on the structure and anchoring of a confined LC film. To do this we present results from full compression sequences performed on a series of systems with substrate region coverages varying in 10% steps from 10% H, 90% P to 90% H, 10% P. In all other respects, these systems are identical to that described in Sec. III. Figure 10 present snapshots of the $\rho^*=0.4$ configurations obtained for this range of systems. These clearly indicate that, depending on the relative proportions of the homeotropic and planar substrate regions, these systems do, indeed, exhibit either a central monodomain or an alternating dual-domain bridging arrangement.

From these snapshots it appears that, for the proportions 10% H and 90% P [Fig. 10(a)], the midfilm part of the system is not significantly influenced by the presence of the homeotropic substrate region and the monodomain formed is equivalent to that of an unpatterned planar-aligned system. This observation also holds for the 20% H and 80% P system [Fig. 10(b)]. It appears, then, that for this film thickness, the

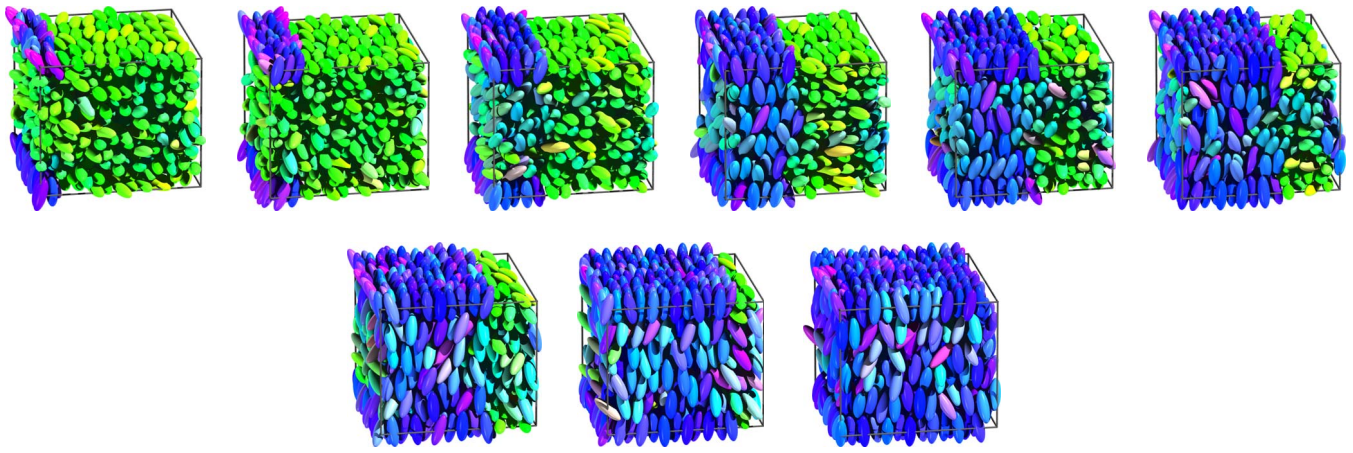

FIG. 10. (Color online) Snapshots of the stripe-patterned system for different coverages of the homeotropic-confining and planar-confining substrate conditions, $\rho^*=0.4$.

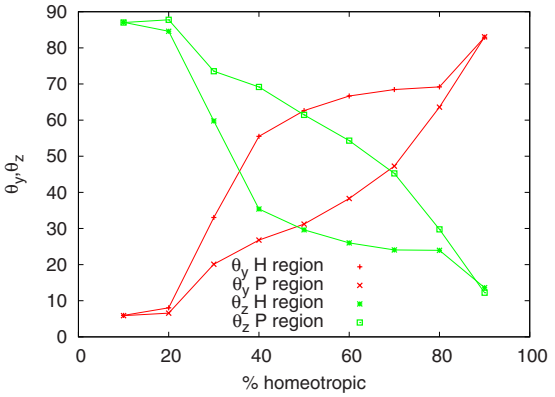

FIG. 11. (Color online) Comparison of θ_y and θ_z values in the two regions.

midfilm structure is insensitive to homeotropic alignment regions of less than $\simeq 30\%$. On the following snapshot [Fig. 10(c)], the system behaves differently. Here, the region confined between the $k_s=0$ surfaces *does* respond to the patterned substrate and the homeotropic alignment region forms a bridged domain across the film.

To substantiate this assessment, we plot, in Fig. 11, the midfilm region-averaged director orientation values θ_y and θ_z corresponding to the two substrate regions. At the limbs of this diagram, where the relative area proportions are poorly balanced, the angles observed coincide, indicating a midfilm monodomain arrangement. Here, the director field is distorted near to the substrates, but the central region forms a single domain whose orientation depends on the relative sizes of the homeotropic and homogeneous substrate regions. Note that for the 80% H system, for which the snapshot in Fig. 10(h) suggests that the thin planar-aligning surface strip has negligible influence, the midfilm anchoring angle is, in fact, tilted due to the substrate patterning. The alternative dual-domain-bridging arrangement, which occurs when the relative surface condition areas are more in balance, corresponds to systems in which the director angles differ in the two regions.

Importantly, the director angle trends observed here cover the full range from planar to homeotropic and, for each domain type, this anchoring angle appears to vary continuously with relative coverage proportion. Figure 11 shows that the tilt angles vary monotonically as the relative stripe width is varied. This suggests that it may be possible to use stripe patterning to achieve *any* desired average director orientation in the midfilm region. Strong azimuthal alignment is found for all of these systems, the midfilm director alignments being effectively pinned to the y-z plane.

V. INFLUENCE OF THE THICKNESS OF THE LIQUID-CRYSTAL FILM

In this section, we investigate the influence of film thickness on the relative stability of the single-domain and dual-bridged-domain structures observed in Sec. IV. We achieve this by considering three further 50% H, 50% P systems with substrate separations $6\kappa\sigma_0$, $7\kappa\sigma_0$, and $8\kappa\sigma_0$. These have been studied using compression sequences of simulations performed with system sizes of 1296, 1512, and 1728 particles, respectively. Other parameters and approaches have been held identical to those used in previous sections, such that, at each density considered, the surface areas of all systems were identical, with only the L_z values varying. High-density snapshots corresponding to these plus the $4\kappa\sigma_0$ system described in Sec. III are represented in Fig. 12. From these, we observe that, as L_z is increased, the domain bridging apparent in the thinnest film becomes increasingly diffuse. To quantify this further we again consider profiles calculated for the two differently confined portions of each system. Selected profiles for the $6\kappa\sigma_0$ and $8\kappa\sigma_0$ are shown in Figs. 13 and 14.

Comparing the Q_{zz} profiles corresponding to the homeotropic region, shown in Figs. 6(c), 13(a), and 14(a), we see that increasing L_z generally leads to a decrease in both the midfilm positional structure and the corresponding Q_{zz} value. Figure 6(c), depicting the Q_{zz} profiles for the nominally homeotropic portion of the $L_z=4\kappa\sigma_0$ system, indicates clear formation of stratified layers both at the surfaces and in the midfilm region. At $\rho^*=0.39$, the average midfilm value of Q_{zz} is about 0.5. The formation of stratified layers is confirmed by the corresponding density profiles [Fig. 4(a)] which show that, away from the substrates, these layers are separated by a distance $\simeq 2.5\sigma_0$. As the thickness of the box

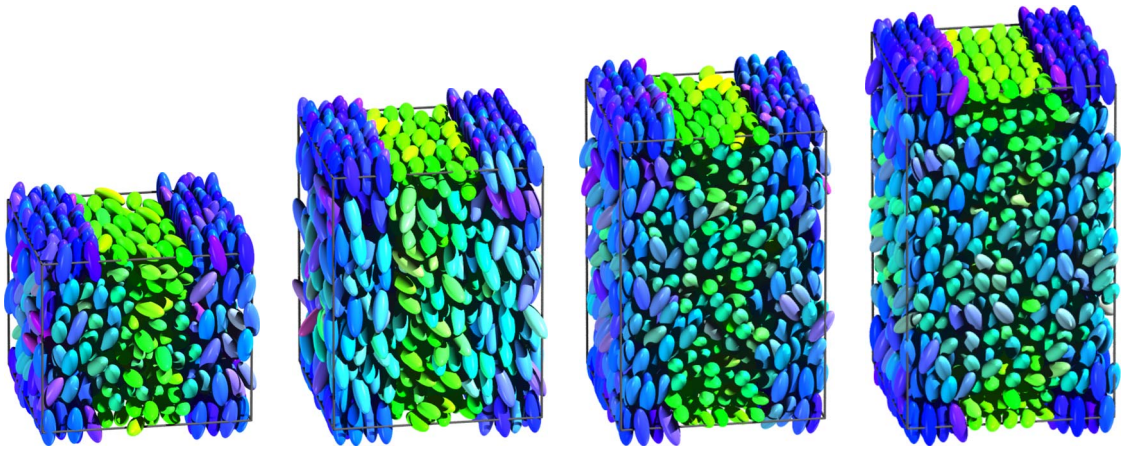

FIG. 12. (Color online) Snapshots of striped systems with different L_z values at $\rho^*=0.4$.

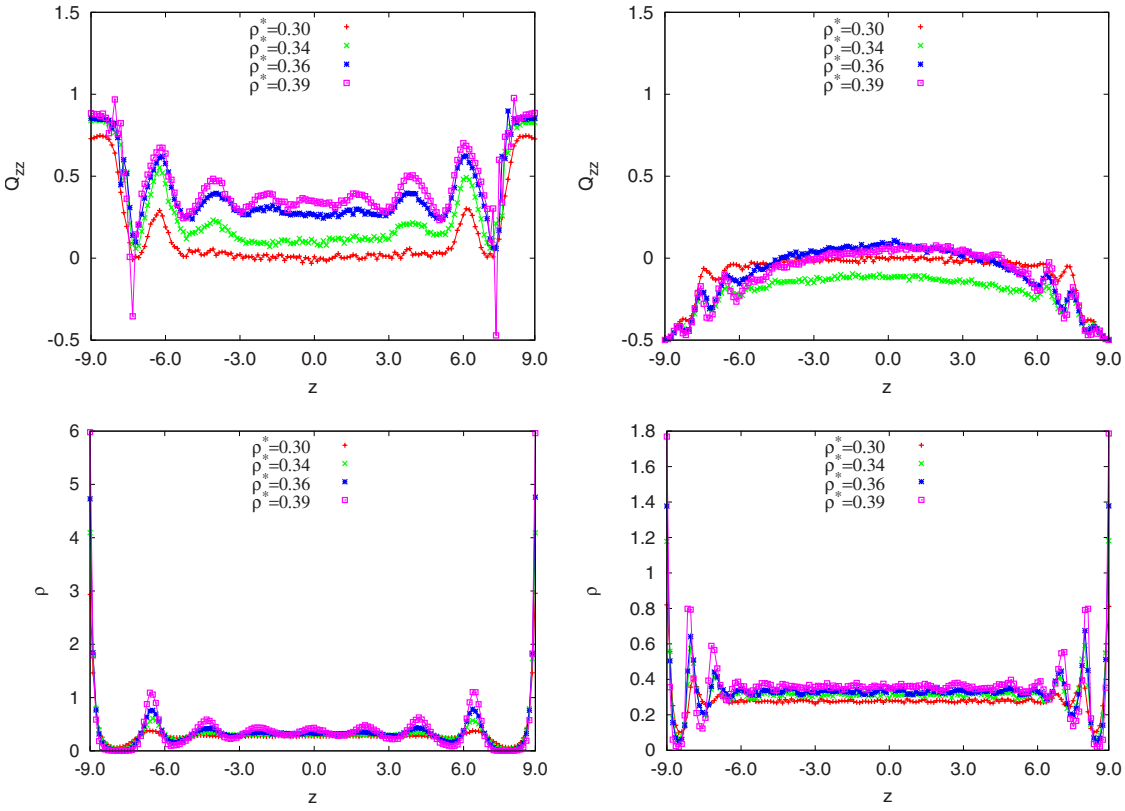

FIG. 13. (Color online) $L_z=6\kappa\sigma_0$: profiles corresponding to the two surface regions.

is increased to $L_z=6\kappa\sigma_0$, the peaks in the homeotropic-region Q_{zz} profiles [Fig. 13(a)] become more damped near the center of the film and the average midfilm value of Q_{zz} $\simeq 0.4$ at $\rho^*=0.4$. Looking at the corresponding density profile [Fig. 13(c)], we can see that there are now seven discernable peaks in addition to the significant surface features. The

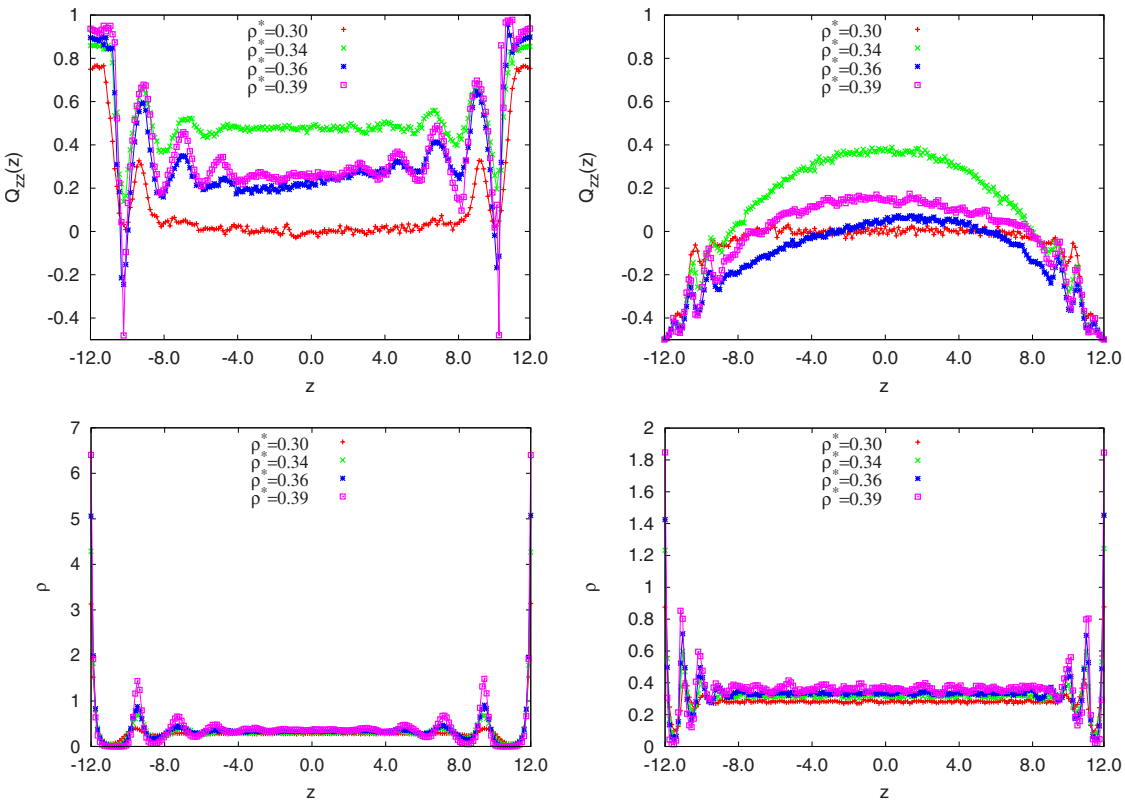

FIG. 14. (Color online) $L_z=8\kappa\sigma_0$: profiles corresponding to the two differently confined subsystems.

distance between the surface monolayers and the second layers is $\simeq 3\sigma_0$, which corresponds to the particle length. The separation distance between subsequent layers is, however, decreased to $\simeq 2\sigma_0$. On increasing the film thickness further to $L_z=8\kappa\sigma_0$, the central region of the homeotropical-confined region loses all positional structure [Figs. 14(a) and 14(c)]. At $\rho^*=0.39$, the latter shows five exponentially damped peaks at each wall. The corresponding Q_{zz} profile [Fig. 14(a)] shows behavior characteristic of the onset of nematic ordering between densities $\rho^*=0.3$ and 0.34, the average value of Q_{zz} rising to about 0.5. However, with further increase in the reduced density to $\rho^*=0.36$, the midfilm Q_{zz} value *decreases* to an average of 0.25 and remains at that level at higher ρ^*.

Recalling the Q_{zz} profile for the planar-confined region of the $L_z=4\kappa\sigma_0$ system [Fig. 7(c)], we can see that its average midfilm value tends to −0.1 at high density. This departs markedly from the behavior of an LC film confined between unpatterned $k_s=3$ substrates, which adopts planar orientations with $Q_{zz}\simeq -0.5$ [16]. As noted above, this difference arises due to the influence of the neighboring homeotropic-confined regions. Unlike what was seen between the homeotropic-confining substrates, however, layering is restricted to the near-surface regions. On increasing the cell thickness to $L_z=6\kappa\sigma_0$, the midfilm Q_{zz} value becomes more negative for a density $\rho^*=0.34$ [Fig. 13(b)]. This is close to the equivalent behavior of a system confined between unpatterned planar-confining substrates. However, as the density is increased further to $\rho^*=0.36$, the midfilm Q_{zz} *increases*, rising to 0.1 and maintaining that value for $\rho^*=0.39$. For the thickest film considered here, alternative nonmonotonic behavior is observed. The Q_{zz} profiles in Fig. 14(b) show that, as the density is increased from 0.3 to 0.34, despite the planar anchoring condition, the midfilm Q_{zz} value is $\simeq 0.4$. This is explained by the behavior of the neighboring homeotropic region: the midfilm Q_{zz} profiles for the two differently confined regions [Figs. 14(a) and 14(b)] both attain this value, showing that the whole of the midfilm exhibits homeotropic anchoring at $\rho^*=0.34$. However, as the density is increased to 0.39, the two midfilm regions both exhibit a drop in Q_{zz} value down to 0.1. This behavior is similar to that seen by Bramble *et al.* [14] in which substrate-patterned systems are dominated by homeotropic alignment at the nematic-isotropic transition but become tilted deeper into the nematic phase window due to the influence of the planar-aligning regions.

To clarify the implications of these order tensor profile observations, we have calculated midfilm director orientations for the four film thicknesses studied. These are plotted in the high-density limit in Fig. 15. This shows, unambiguously, that the high-density $Q_{zz}(z)$ profiles for the thickest films correspond to the onset of significant midfilm director tilt. The midfilm tilt values obtained in the differently confined regions are clearly different from one another for the thinnest film but converge as the film thickness is increased. This observation is in good agreement with the original inference from the snapshots in Fig. 12—increasing the film thickness leads to breakdown of the dual-bridged-domain arrangement in favor of a tilted central monodomain.

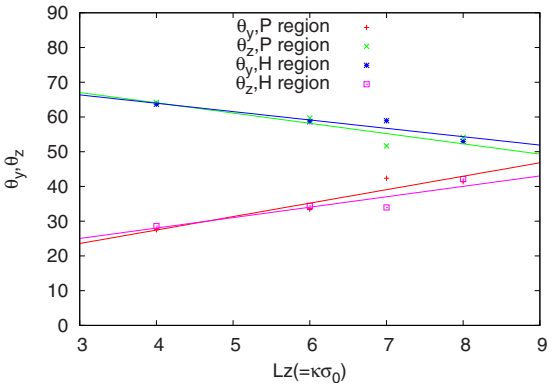

FIG. 15. (Color online) Variation of θ_y and θ_z in the homeotropic-confined (H) and planar-confined (P) regions for different film thicknesses L_z.

VI. CONCLUSIONS

In this paper, we have presented a comprehensive simulation study of thin LC films confined between stripe-nanopatterned substrates. In these, we have concentrated on the influence of two parameters: the relative stripe width and the cell thickness, with a view to establishing the molecular mechanisms that underpin the device-scale and continuum-level behaviors of such systems. From these, we have shown that the relative stripe width is crucial in determining the polar anchoring angle adopted in the midfilm region. Importantly, there appears to be a monotonic relationship between the relative stripe width and this bulk tilt angle. As a consequence, we predict that, provided the very thin-film limit is avoided, tilted LC monodomains with any desired polar anchoring angle can be obtained using systems of this geometry, the angle adopted being controlled by the relative stripe width. Due to the fact that the relative influence of the planar and homeotropic substrate regions changes significantly as nematic order develops in these systems, however, bulk tilt is *not* expected to develop at T_{NI} but rather to be delayed to lower temperatures. This is identical to what is observed experimentally in systems with a single stripe-patterned substrate [14].

For very thin films, we have observed bridged domains of different orientation traversing the full film width. Taking our HGO particles as typical mesogens of length 2–3 nm, our results indicate that bridging should only be seen experimentally on films of thickness 10–20 nm. Deep in the nematic phase, the orientations adopted by these domains have been shown to be partial tilts, adopted as a compromise between the local substrate condition and the neighboring domain orientation. Increasing film thickness leads to a decay of this bridging arrangement, such that a single tilted monodomain becomes the dominant configuration. For all systems studied, we have observed discontinuous orientational crossover between planar and homeotropic surface pretilt states. These discontinuous boundaries at the substrate become diffuse domain walls in the interfacial LC region, however, and become undetectable a few molecular lengths from the substrate. The persistence of these domain walls is the crucial parameter in determining the stability of the bridging ar-

rangement. We have not seen any evidence that these domain walls are influenced by the lateral breadth of the stripe patterning, so we do not expect bridging arrangements to be seen in micron thickness films even given, e.g., increase in the patterning wavelength. Further, we would not expect them to feature in continuum-scale modeling of systems with pretilt discontinuities.

Stripe patterning imposes a strong azimuthal anchoring condition for all of the systems we have considered here. This is consistent with established experimental behavior in such systems. Our results clearly indicate that this azimuthal anchoring develops due to the sharp pretilt orientational discontinuities that spontaneously form at the boundaries of the substrate patterns. In addition to the systems presented above, we have investigated the influence of diffuse substrate condition boundaries (i.e., linear variation in k_s rather than sharp changes) [21]. Such behavior can be achieved experimentally using mixed or photocleaving SAM-coated substrates. In practice, however, even when the substrate condition is smoothed, the substrate region alignment adopted in the simulated system shows a molecularly sharp discontinuity in the pretilt orientation. Given the robustness of these features and their importance for establishing azimuthal alignment, we predict that the continuum anchoring coefficient should vary in proportion to their density, i.e., the stripe inverse wavelength. We *have* found that fundamentally different behaviors can be observed in related systems based on two-dimensional patternings such as squares, rectangles, and circles. These will be reported in full in a future publication.

ACKNOWLEDGMENTS

This work was supported by the Engineering and Physical Research Council, Grant No. GR/S59833/01. We acknowledge useful conversations with Steve Evans, Jim Henderson, Jon Bramble, Chris Care, Tim Spencer, and Paulo Teixeira which have been beneficial to our understanding of the systems studied here.

[1] B. Jérôme, Rep. Prog. Phys. **54**, 391 (1991).
[2] C. V. Brown, M. J. Towler, V. C. Hui, and G. P. Bryan-Brown, Liq. Cryst. **27**, 233 (2000).
[3] S. Kitson and A. Geisow, Appl. Phys. Lett. **80**, 3635 (2002).
[4] J. H. Kim, M. Yoneya, and H. Yokoyama, Nature (London) **420**, 159 (2002).
[5] D. W. Berreman, Phys. Rev. Lett. **28**, 1683 (1972).
[6] T. Z. Qian and P. Sheng, Phys. Rev. Lett. **77**, 4564 (1996).
[7] T. Z. Qian and P. Sheng, Phys. Rev. E **55**, 7111 (1997).
[8] S. Park, C. Padeste, H. Schift, J. Gobrecht, and T. Scharf, Adv. Mater. **17**, 1398 (2005).
[9] T. Scharf, S. Park, C. Padeste, H. Schift, N. Basturk, and J. Grupp, Mol. Cryst. Liq. Cryst. **438**, 1619 (2005).
[10] B. Lee and N. A. Clark, Science **291**, 2576 (2001).
[11] R. A. Drawhorn and N. L. Abbott, J. Phys. Chem. **99**, 16511 (1995).
[12] Y. L. Cheng, D. N. Batchelder, S. D. Evans, J. R. Henderson, J. E. Lydon, and S. D. Ogier, Liq. Cryst. **27**, 1267 (2000).
[13] I. H. Bechtold and E. A. Oliveira, Liq. Cryst. **32**, 343 (2005).
[14] J. P. Bramble, S. D. Evans, J. R. Henderson, C. Anquetil, D. J. Cleaver, and N. J. Smith, Liq. Cryst. **34**, 1059 (2007).
[15] P. Padilla and E. Velasco, J. Chem. Phys. **106**, 10299 (1997).
[16] D. J. Cleaver and P. I. C. Teixeira, Chem. Phys. Lett. **338**, 1 (2001).
[17] F. Barmes and D. J. Cleaver, Phys. Rev. E **69**, 061705 (2004).
[18] M. Schoen and D. J. Diestler, Chem. Phys. Lett. **270**, 339 (1997).
[19] M. Schoen, Phys. Chem. Chem. Phys. **10**, 223 (2008).
[20] S. Kondrat, A. Poniewierski, and L. Harnau, Eur. Phys. J. E **10**, 163 (2003).
[21] C. Anquetil-Deck, Ph.D. thesis, Sheffield Hallam University, 2008.